Microstructural dynamics of central uplifts: Reidite off-set by zircon twins at the Woodleigh impact structure, Australia

Morgan A. Cox[1*], Aaron J. Cavosie[1], Phil A. Bland[1], Katarina Miljković[1], and Michael T. D. Wingate[2]

[1]*Space Science and Technology Centre (SSTC), School of Earth and Planetary Science, Curtin University, Perth, WA 6102, Australia*

[2]*Geoscience and Resource Strategy Division, Department of Mines, Industry Regulation and Safety, Perth, WA 6004, Australia*

*E-mail address: morgan.cox@student.curtin.edu.au

Contents

Item DR1. Sample location and preparation

Location of the sample:
The sample was recovered from the 294.3–295.2 m depth interval of the Woodleigh-1 drill core, which penetrated the central uplift of the Woodleigh impact crater, at latitude 26°03'19.3"S and longitude 114°39'56.3"E.

Preparation of the sample:
The core sample was crushed and zircon grains were separated using standard magnetic and high-density liquid techniques (e.g. Wingate and Lu, 2017). Zircon grains were hand-picked and cast in an epoxy mount, which was polished to expose the interiors of the crystals for imaging by optical and cathodoluminescence (CL) techniques. The mount was subsequently polished to EBSD standard using collodial silica and carbon coated.

Survey techniques:
A Tescan MIRA 3 field emission scanning electron microscope (SEM) at Curtin University was used to collect detailed BSE and CL images of individual zircon grains. EBSD maps were then collected for 16 zircon grains. Whole-grain maps ranged in step size from 100 to 600 nm. EBSD imaging employed an accelerating voltage of 20 kV, a working distance of 20.5 mm, and a beam intensity of 18 nA. The sample was tilted at 70° and the EBSD patterns were collected using a Nordlys Nano high-resolution detector along with the Oxford Instruments Aztec system. Tango and Mambo modules in the software package Oxford Instruments/HKL Channel 5 were used to process EBSD maps collected.

Item DR2. Image of core sample GSWA 199093, from which zircons were seperated

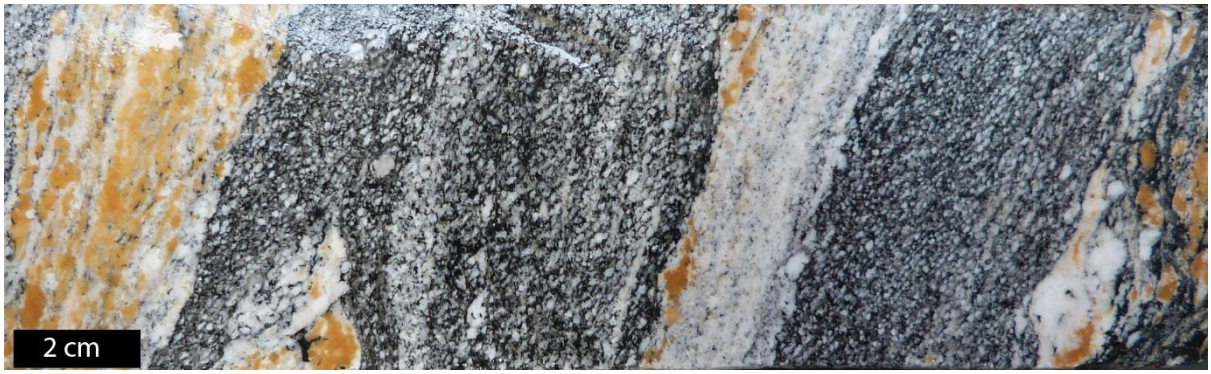

Item DR3. Petrographic description, GSWA 199093: monzogranitic gneiss

The sample is a fine- to medium-grained gneiss of monzogranitic composition, consisting of about 25% plagioclase, 25% K-feldspar, 20% quartz, 20% biotite, and minor muscovite, iron-titanium oxide minerals, epidote, clinozoisite, and zircon. Plagioclase (andesine, An_{43}) occurs as ribbons of albite-twinned grains up to 4 mm long that are incipiently saussurite altered. K-feldspar (microcline) grains are up to 2 mm across. Quartz forms mosaics of grains up to about 1 mm across, intermeshed with well aligned biotite grains up to 1 mm long. Feldspars and quartz have been shock metamorphosed, such that feldspar exhibits strain shadows and contains strings of inclusions that obscure twin lamellae, and quartz displays planar deformation features (PDFs). The focus of this study did not involve indexing of shocked quartz, however Reimold et al. 2003 have published shocked quartz data at depths above and below this sample with PDF orientations in grains. The measured PDF orientations include $\{10\bar{1}3\}$, $\{10\bar{1}2\}$ and $\{21\bar{3}1\}$ at 272 m depth and $\{10\bar{1}3\}$ and $\{10\bar{1}2\}$ at 326.7 m depth which indicates shock pressures ~15-25 GPa.

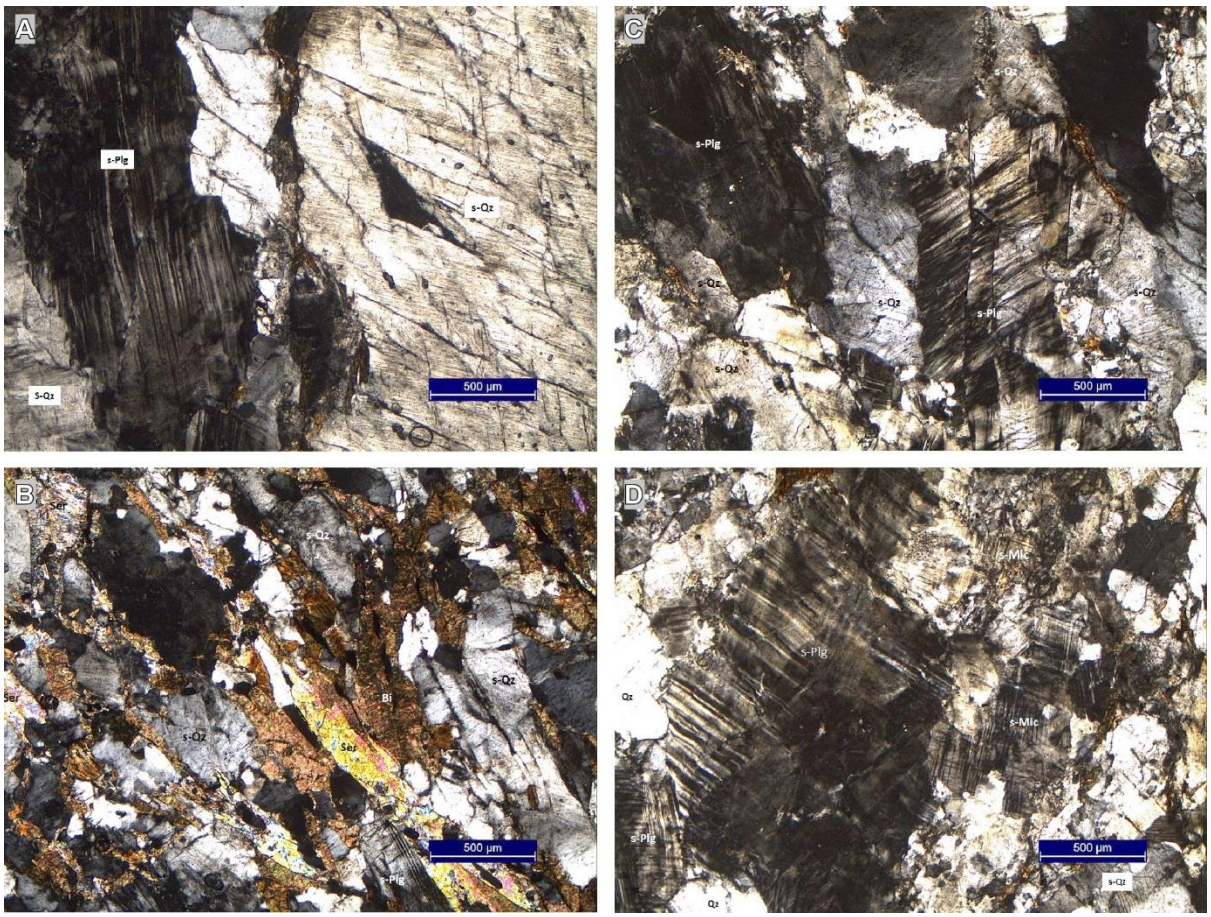

Optical photomicrographs (crossed polarized light) of sample GSWA 199093, monzogranitic gneiss. Abbreviations: Qz, quartz; Plg, plagioclase; Mic, microcline; Bi, biotite; Ser, sericite; s-, showing evidence of shock metamorphism.

Item DR4. Back-scattered electron (BSE) and cathodoluminescence (CL) images of zircon grains 112 and 103-1. Both grains contain reidite lenses that are offset by {112} deformation twins.

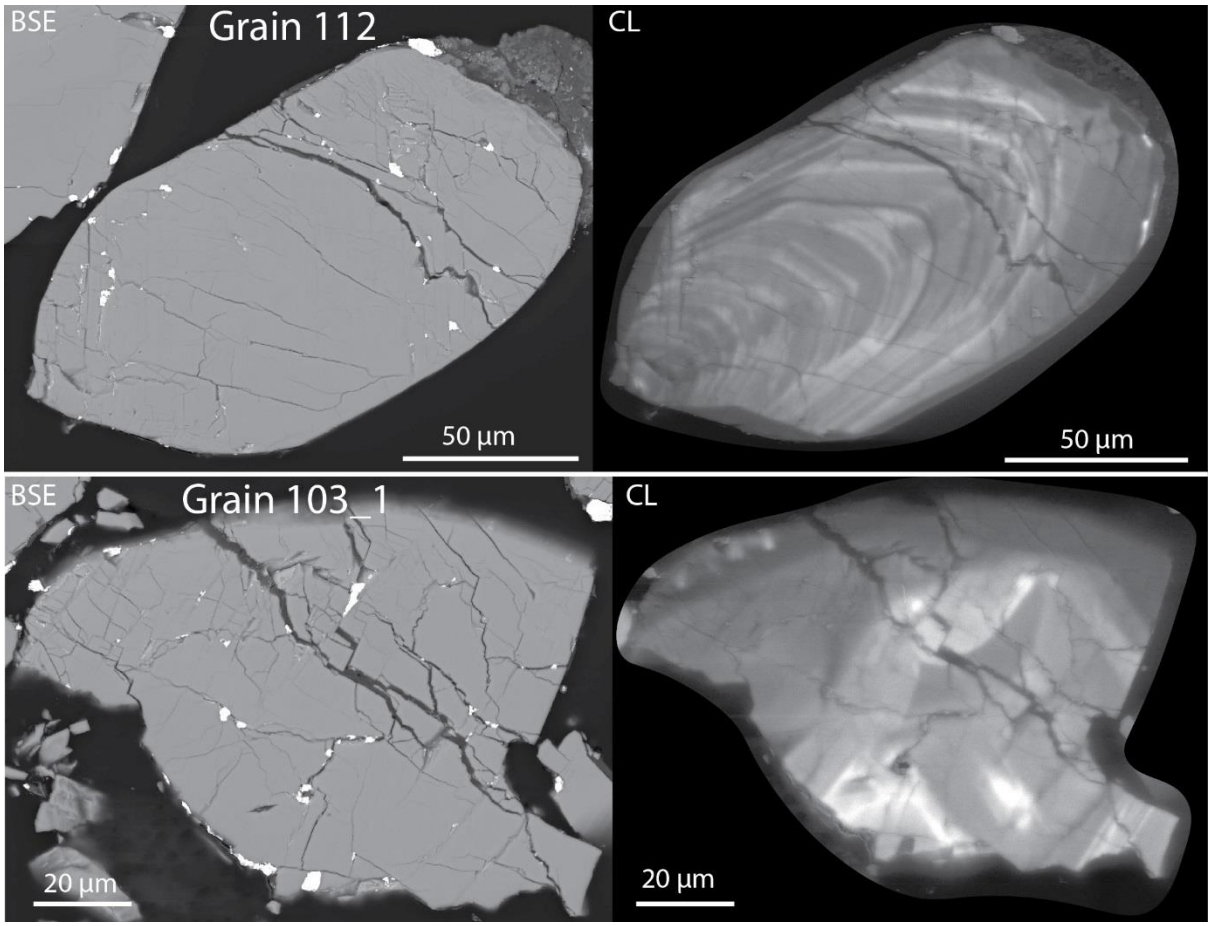

Item DR5. Electron backscatter diffraction (EBSD) data for zircon grain 103-1. A) Whole-grain inverse pole figure of zircon grain containing reidite which has an apparent offset along {112} deformation twins. B) ROI of reidite which is offset by {112} deformation twin. C) Pole figure showing orientation of host zircon, reidite and zircon twin. BC= band contrast, IPF= inverse pole figure.

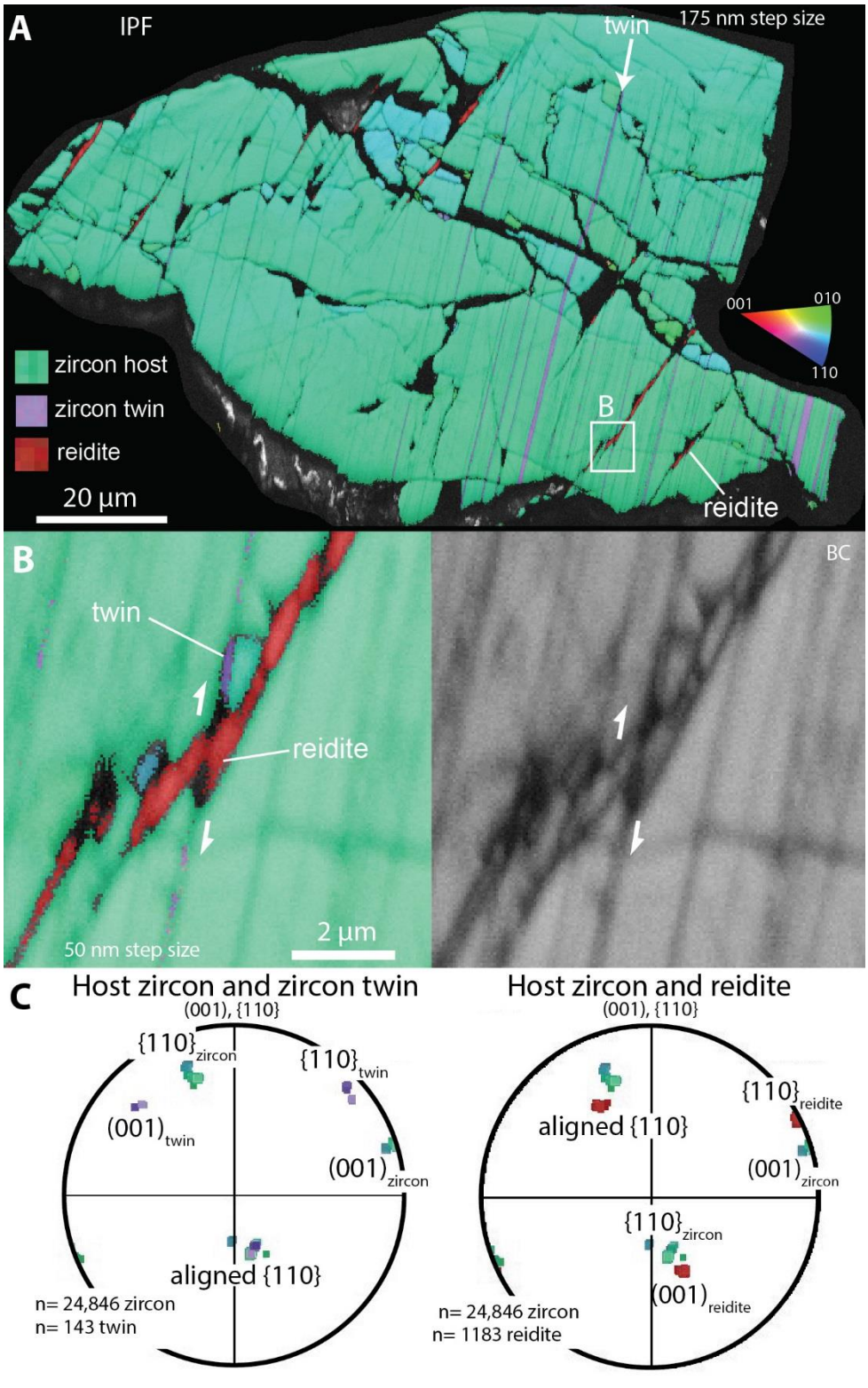

Item DR6. BSE, CL and EBSD images of four zircon grains which contain reidite and {112} deformation twins (zircon= blue, twin= red, reidite= yellow).

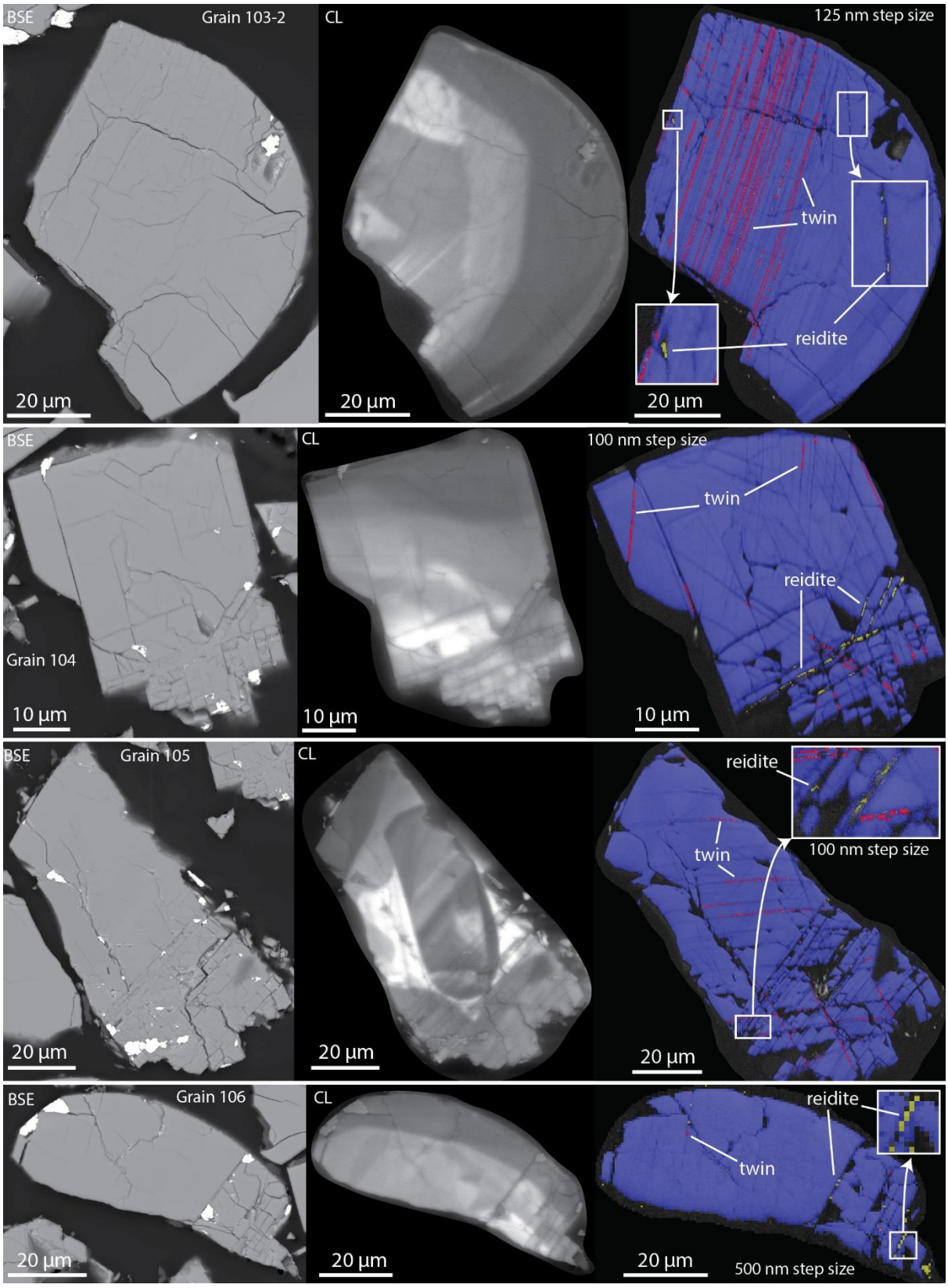

Item DR7. BSE, CL and EBSD images of five zircon grains which contain reidite, but no {112} twins (zircon= blue, reidite= yellow).

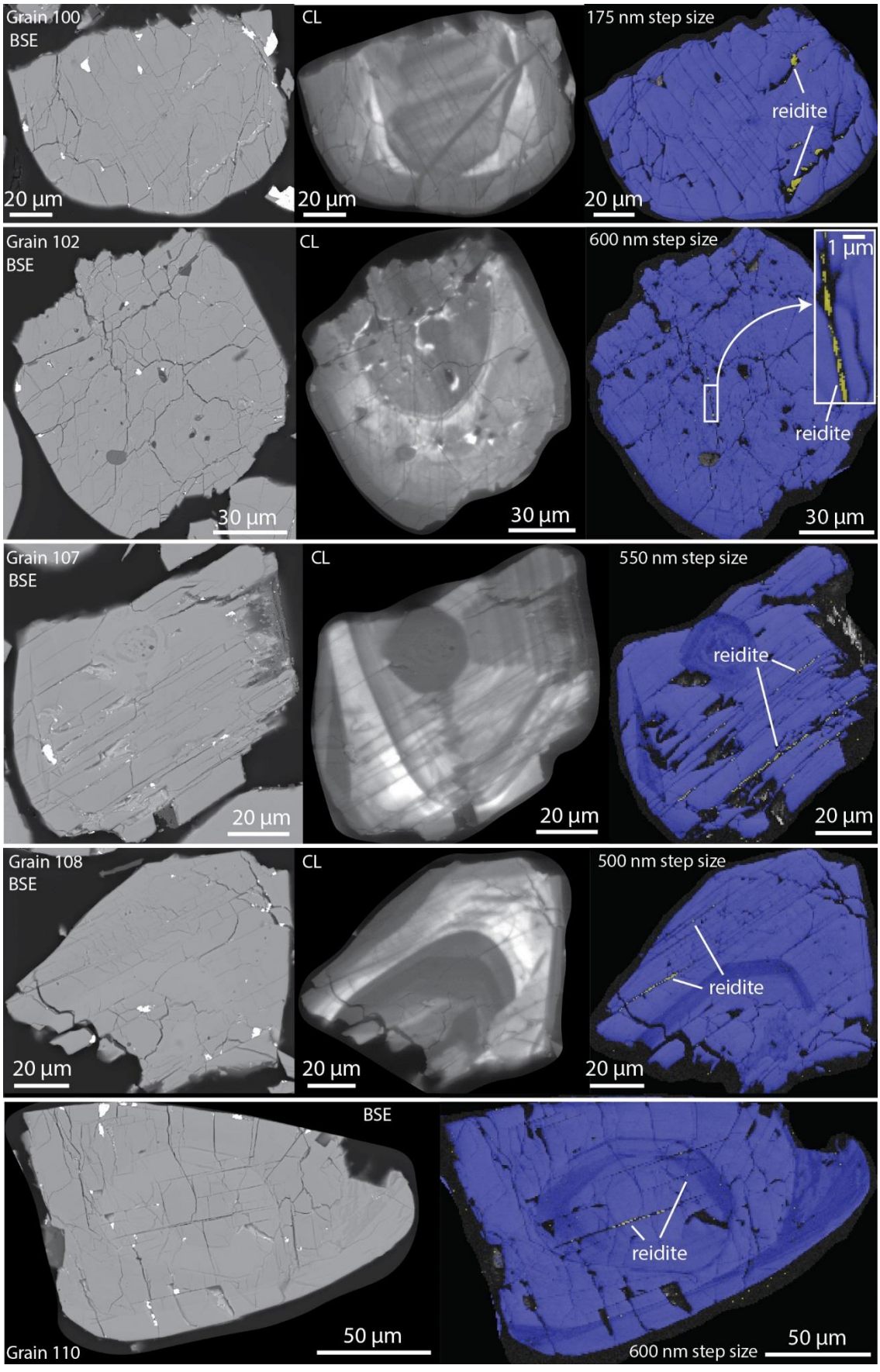

Item DR8. Numerical impact modelling: method and results.

The iSALE shock physics hydrocode (Amsden et al. 1980; Collins et al. 2004; Wünnemann et al. 2006) was used to model the formation of the Woodleigh structure in order to determine the shock-level of material within the central uplift. Considering the uncertainty in the crater size, for the purpose of this work, we model it as a 90-km diameter crater, which is in between the estimates previously made by Reimold et al. (2003) and Glikson et al. (2005). Simulations of a 60-km crater and 120-km crater yield similar results, for the purpose of Figure 3.

The cell resolution in a 2D numerical mesh was 200 by 200 m and 20 CPPR. (CPPR stands for "Cells Per Projectile Radius" and is a measure of computational accuracy. This level of CPPR is appropriate for this simulation.) This means that the projectile used in the simulation was 8 km in diameter, impacting Earth at 12 kms-1 vertical speed; this speed also represents faster speeds at moderately oblique impact angles (e.g., Pierazzo and Melosh 2000). The impactor was modelled using the analytical equation of state (ANEOS) for dunite (Benz et al. 1989) representative of a stony asteroid. The target rocks at Woodleigh are granitic non-porous basement, therefore the target was simulated using the ANEOS equation of state for granite (Pierazzo et al. 1997). Other parameters used in this iSALE impact simulation are adopted from the iSALE simulation made for the formation of the Chicxulub crater (Collins et al., 2002).

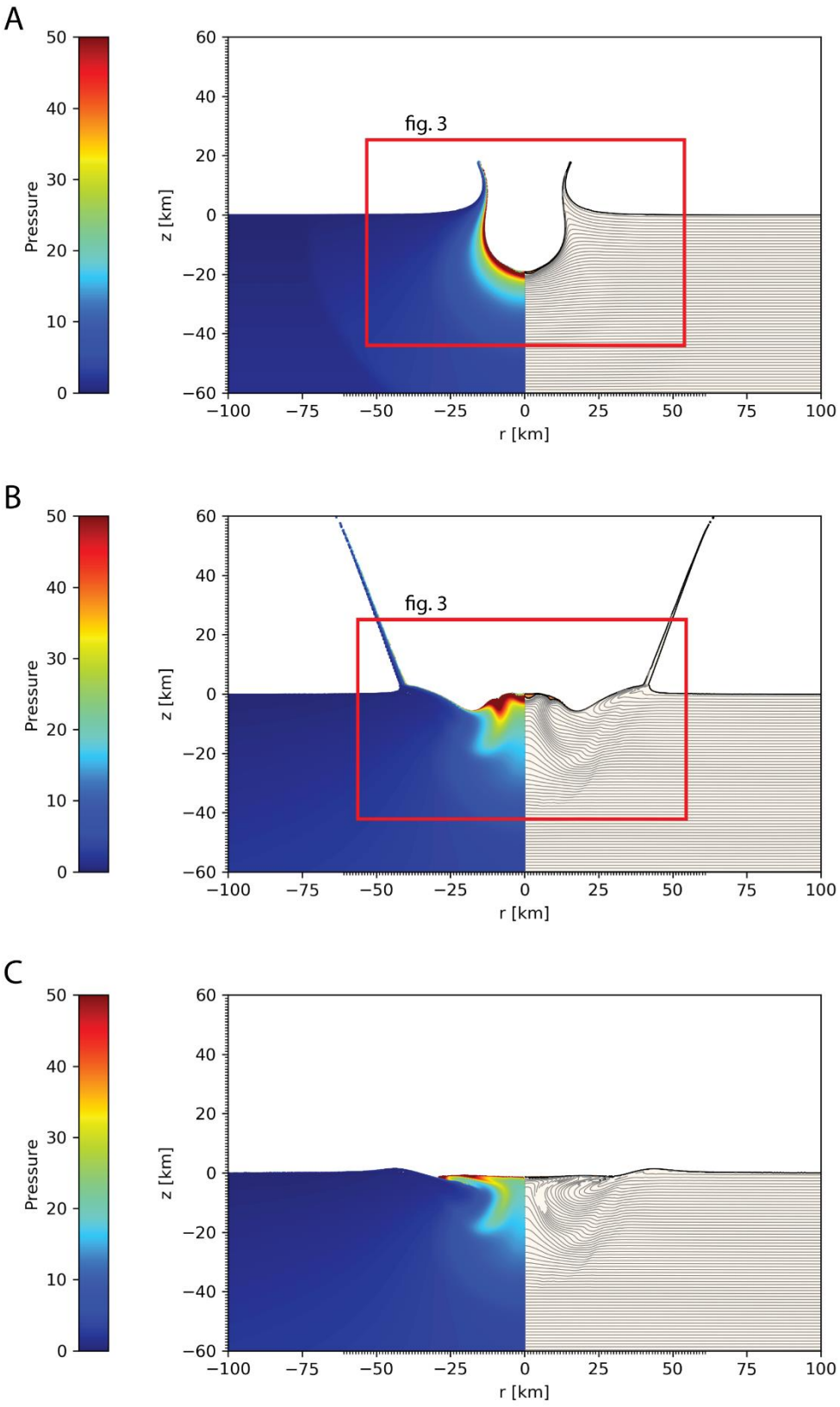

Above: Numerical simulation of the Woodleigh impact structure. Peak pressure is shown on the left and material displacement is shown on the right (r = radius, z = height relative to the paleo surface). Panels A and B contain red boxes which indicate the insets used in Figure 3. Panel C shows the final crater diameter of Woodleigh (90 km).

Data Repository References

Amsden A. A., Ruppel H. M., and Hirt C. W. 1980. SALE: A Simplified ALE Computer Program for Fluid Flow at all Speeds. Report LA-8095. Los Alamos National Laboratories, N. Mex. 105 pp.

Benz W., Cameron A. G. W., and Melosh H. J. 1989. The Origin of the Moon and the single-impact hypothesis III. Icarus 81:113-131.

Collins G. S., Melosh H. J., Morgan Jo V., and Warner M. R. 2002. Hydrocode Simulations of Chicxulub Crater Collapse and Peak-Ring Formation. Icarus 157, 24—33.

Collins G. S., Melosh H. J., and Ivanov B. A. 2004. Damage and Deformation in Numerical Impact Simulations. Meteoritics & Planetary Science 39:217–231.

Pierazzo E. and Melosh H. J. 2000. Understanding Oblique Impacts from Experiments, Observations, and Modelling. Annual Reviews in Earth and Planetary Science 28:141–167.

Pierazzo E., Vickery A. M., and Melosh H. J. 1997. A reevaluation of impact melt production. Icarus 127:408–423.

Wingate, M.T.D., and Lu, Y., 2017, Introduction to geochronology information 2017: Geological Survey of Western Australia, 5p.

Wünnemann K., Collins G. S., and Melosh H. J. 2006. A Strain-Based Porosity Model for Use in Hydrocode Simulations of Impacts and Implications for Transient Crater Growth in Porous Targets. Icarus 180:514–527.